


RESEARCH ARTICLE

Lysine methyltransferase 2D regulates muscle fiber size and muscle cell differentiation

Alec Wright¹ | Arielle Hall¹ | Tara Daly^{1,2} | Tatiana Fontelonga¹ | Sarah Potter³ | Caitlin Schafer³ | Andrew Lindsley^{3,4} | Christina Hung^{1,2} | Olaf Bodamer^{1,2,5} | Emanuela Gussoni^{1,2,6} 

¹Division of Genetics and Genomics, Boston Children's Hospital, Boston, Massachusetts, USA

²The Royce Kabuki Program, Boston Children's Hospital, Boston, Massachusetts, USA

³Division of Allergy and Immunology, Cincinnati Children's Hospital, Cincinnati, Ohio, USA

⁴Amgen, Thousand Oaks, California, USA

⁵Division of Genetics and Genomics, Broad Institute of MIT and Harvard University, Cambridge, Massachusetts, USA

⁶The Stem Cell Program, Boston Children's Hospital, Boston, Massachusetts, USA

Correspondence

Emanuela Gussoni, Division of Genetics and Genomics, Boston Children's Hospital, 3 Blackfan Circle 15021, Boston, MA 02115, USA. Email: emanuela.gussoni@enders.tch.harvard.edu

Funding information

Royce Kabuki Program; NIH/NIAMS, Grant/Award Number: 1R01AR069582 (EG)

Abstract

Kabuki syndrome (KS) is a rare genetic disorder caused primarily by mutations in the histone modifier genes *KMT2D* and *KDM6A*. The genes have broad temporal and spatial expression in many organs, resulting in complex phenotypes observed in KS patients. Hypotonia is one of the clinical presentations associated with KS, yet detailed examination of skeletal muscle samples from KS patients has not been reported. We studied the consequences of loss of *KMT2D* function in both mouse and human muscles. In mice, heterozygous loss of *Kmt2d* resulted in reduced neuromuscular junction (NMJ) perimeter, decreased muscle cell differentiation in vitro and impaired myofiber regeneration in vivo. Muscle samples from KS patients of different ages showed presence of increased fibrotic tissue interspersed between myofiber fascicles, which was not seen in mouse muscles. Importantly, when *Kmt2d*-deficient muscle stem cells were transplanted in vivo in a physiologic non-Kabuki environment, their differentiation potential is restored to levels undistinguishable from control cells. Thus, the epigenetic changes due to loss of function of *KMT2D* appear reversible through a change in milieu, opening a potential therapeutic avenue.

KEYWORDS

Kabuki syndrome, muscle differentiation, muscle regeneration, muscle stem cells, muscular dystrophy, NMJ

Abbreviations: ASCOM, activating signal co-integrator-2 (ASC-2) complex; bFGF, basic fibroblast growth factor; FBS, fetal bovine serum; H3K4me1, histone 3 lysine 4 monomethyl; KDM6A, lysine demethylase 6A; KMT2D, lysine methyltransferase 2D; KS, Kabuki syndrome; NMJ, neuromuscular junction; PBS, phosphate buffered saline; Pen/strep, penicillin/streptomycin; WT, wildtype; α -BTX, alpha bungarotoxin.

This work was partially supported by NIH/NIAMS 1R01AR069582 (EG)

This is an open access article under the terms of the Creative Commons Attribution-NonCommercial-NoDerivs License, which permits use and distribution in any medium, provided the original work is properly cited, the use is non-commercial and no modifications or adaptations are made.

© 2021 The Authors. *The FASEB Journal* published by Wiley Periodicals LLC on behalf of Federation of American Societies for Experimental Biology

1 | INTRODUCTION

Kabuki Syndrome (KS) is a rare disease caused by heterozygous mutations in *KMT2D* (KS-1; OMIM#147920) and *KDM6A* (KS-2; OMIM# 300867). The genes encode for histone modifier proteins that regulate gene expression of downstream targets.¹ Specifically, *KMT2D* is known to induce gene activation both via addition of H3K4me1 activation marks at target gene promoters/enhancers, as well as via enzymatic-independent mechanisms.^{2,3} Similarly, *KDM6A* (also called UTX) is known to activate gene transcription via removal of repressive H3K27me3 marks,⁴ although gene regulation via demethylase-independent activity has also been reported.⁵ Patients affected by KS present with a variable, multi-systemic clinical phenotype, including, but not limited to intellectual disability, developmental delays, hearing loss, hypotonia, cardiac and renal anomalies, as well as short stature.⁶ This broad spectrum of clinical findings and phenotype severity can be partially attributed to the widespread expression of the *KMT2D* and *KDM6A* genes in multiple organs, which span temporally from embryonic development through postnatal life. *KMT2D* and *KDM6A* proteins are linked functionally, as they are part of the large Activating Signal Co-integrator-2 (ASC-2)/NCOA6 (ASCOM) protein complex.⁷ Specifically, *KMT2D* seems to be a crucial component for the organization of this protein complex and loss of *KMT2D* protein in cells results in impaired complex formation and destabilization of *KDM6A* activity.^{8–10}

Conditional and non-conditional mouse models for KS have been generated to study the consequences of constitutive heterozygous or tissue-specific loss of function of *KMT2D* and *KDM6A*.^{11–15} One mouse model that has been proven useful to study human KS is the constitutive *Kmt2d*^{+/β^{Geo}}.¹¹ In this model, *Kmt2d* expression is driven only by one allele, while the second allele is disrupted by a β^{Geo} cassette insertion, thus genetically resembling human KS etiology.¹¹

One of the common symptoms associated with KS is skeletal muscle hypotonia, affecting both proximal and distal muscle groups.^{16–18} Previous studies in mice have documented that both *Kdm6a* and *Kmt2d* play an active role in regulating skeletal muscle cell differentiation. In muscle cells, *Kdm6a* activates the myogenic transcription factor *myogenin*,¹⁹ an early driver of muscle differentiation that mediates cell fusion and formation of syncytial myofibers. Importantly, mice with depleted *Kdm6a* expression in Pax7-expressing muscle stem cells showed impaired differentiation and poor myofiber regeneration in vivo.¹² More recently, specific ablation of *Kmt2d* in myofibers resulted in severe loss of Type I (slow) muscle fibers in the soleus and gastrocnemius muscles caused by impaired MEF2C activation, a downstream target of *Kmt2d*.¹⁵

Whether hypotonia in human KS is due to primary skeletal muscle abnormalities, including decreased muscle

stem cell activity and/or decreased muscle fiber size is currently unknown. We sought to examine whether hypotonia in KS arises from a primary deficiency of skeletal muscle cells using the *Kmt2d*^{+/β^{Geo}} mouse model and muscle samples from KS patients. Young (3 weeks) *Kmt2d*^{+/β^{Geo}} mice displayed a significant reduction in myofiber size, which was overcome in adulthood (age 4 and 10 months). Ten-month-old mice presented a significant reduction in neuromuscular junction (NMJ) perimeter, but no significant difference in branch number or length. In human muscle, variable presence of intramuscular fibrosis was observed in all samples, which was not noted in the mouse model. Muscle stem cells from *Kmt2d*^{+/β^{Geo}} mice exhibited delayed/impaired differentiation in vitro, marked by significantly decreased expression of myogenin and decreased fusion. Furthermore, when muscles of WT and *Kmt2d*^{+/β^{Geo}} mice were acutely injured and induced to regenerate, newly formed myofibers were significantly smaller in *Kmt2d*^{+/β^{Geo}} mice. To determine if this delay/deficiency in differentiation is irreversible, primary satellite cells (muscle stem cells) extracted from WT and *Kmt2d*^{+/β^{Geo}} muscles were transplanted in vivo into a physiologic non-Kabuki environment. Analyses of these transplants showed that WT and *Kmt2d*^{+/β^{Geo}} donor muscle stem cells provided similar engraftment yields. These studies demonstrate that any potential differentiation defect observed in *Kmt2d*^{+/β^{Geo}} cells is not embryonically determined and can be reversed postnatally through environmental changes.

2 | MATERIALS AND METHODS

2.1 | Human samples

Excess muscle tissue from orthopedic procedures was collected into Dulbecco's modified Eagle Medium (DMEM) with high glucose and supplemented with 20% fetal bovine serum and antibiotics (penicillin/streptomycin) for overnight shipment, following informed written consent. Immediately upon arrival at Boston Children's Hospital, muscle samples were either frozen in cold isopentane for histology analyses²⁰ or dissociated and digested for satellite cell (muscle stem cells) isolation. Human muscle satellite cells were dissociated in a cocktail of Dispase II and collagenase D and purified as previously described.^{21,22} All experiments involving human material were approved by the Boston Children's Hospital (Boston, MA) Institutional Review Board (IRB-P00026691) and conducted in accordance with the IBC Institutional Regulations at Boston Children's Hospital, Boston, MA. Consented patients had a confirmed clinical diagnosis of KS and a confirmed pathogenic mutation in the *KMT2D* gene in 4 of 5 patients. The age of the patients ranged between 6 months and 13 years, with one post-mortem case.

Control tissue was obtained as de-identified, discarded tissue as approved by the Boston Children's Hospital Institutional Review Board (IRB-P00020286).

2.2 | Mouse models

B6;129P2-*Kmt2d*^{Gt(RRT024)Byg}/Mmucd mutant mice (also named *Kmt2d*^{+/β^{Geo}}) were originally generated by BayGenomics and have been extensively used in previous studies as a model for KS.^{11,13,23,24} The mice are heterozygous mutants in the *Kmt2d* locus and therefore genetically model patients with KS. Three-weeks, 6 and 10 months old male and female WT and *Kmt2d*^{+/β^{Geo}} mice were analyzed in these studies. Two-month-old Rag1^{null} mdx^{5cv} female mice lacking the protein dystrophin were used as recipients in transplantation assays.²⁵ All experiments involving vertebrate animals were approved and conducted in accordance with IACUC Institutional Regulations at Boston Children's Hospital, Boston, MA and Cincinnati Children's Hospital, OH. Cohorts of littermate animals (at least $n = 5-6$ mice/genotype) were used for each experiment and equal numbers of male and female animals were used in each cohort.

2.3 | Mouse graded maximal exhaustion treadmill test

The treadmill exercise test was performed as previously described²⁶ on a 6-line motorized treadmill with adjustable speed, inclination, and equipped with an electric shock-delivering grid (Columbus Instruments, Columbus, OH, USA). All mice were pre-acclimatized to experimental settings the day prior by running for 15 min at a speed of 10 m/min with disabled electric shock-delivering grid without an incline. During the test, the non-incline treadmill program consisted of 5 min of warm-up at 5 m/min and then step-wise increased to 25 m/min. Electric shock intensity was set to 1 mA. Each mouse was allowed to continue until exhaustion, determined as when the mouse would rather receive the shock than run. This was experimentally defined as when the hind limbs or body rested continuously on the shock pad for three seconds on three separate occasions. At exhaustion, the total distance each mouse ran was recorded.

2.4 | Histology and immunofluorescence analyses on muscle tissue sections

2.4.1 | H&E staining

8 μm frozen muscle tissue sections were placed on slides and processed as previously described.²⁷ All slides were

imaged on a brightfield Nikon E800 microscope (Nikon, Melville, NY, USA, RRID:SCR_020326) using SPOT software (Diagnostic Instruments, Sterling Heights, MI, United States, RRID:SCR_014313). Entire sections were photomerged and fiber measurements were analyzed using FIJI (NIH, Bethesda, MD, USA, RRID:SCR_002285). Statistical analyses were done using Microsoft Excel (Microsoft Corporation, Redmond, WA, USA, RRID:SCR_016137) and GraphPad Prism 9 (GraphPad Software, San Diego, CA, USA, RRID:SCR_002798).

2.4.2 | Fiber type staining

8 μm frozen sections were collected from mouse and human muscle tissues and allowed to air dry for 30 min. Sections were blocked for 40 min in 1X PBS with 5% goat serum at room temperature. Primary antibodies were obtained from the Developmental Studies Hybridoma Bank (DSHB, University of Iowa, Iowa City, IA, USA): BA-D5-s (IgG2b, 1:50 dilution, RRID:AB_2235587) for MyHC-1, SC-71-c (IgG1, 1:500, RRID:AB_2147165) for MyHC-2A, BF-F3-c (IgM, 1:100, RRID:AB_2266724) for MyHC-2B, laminin (LS-C96142, 1:500, LS Bio, Seattle, WA, USA, RRID:AB_2134058) was used to outline the fibers. Primary antibodies were diluted in blocking solution and incubated at 37°C for 1 h. Following 3 × 5 min washes in 1X PBS, secondary antibodies (goat anti-mouse IgG2b DyLight405, RRID:AB_2632531, goat anti-mouse IgG1 Alexa Fluor 488, RRID:AB_2632534, goat anti-mouse IgM Alexa Fluor 594, RRID:AB_2338901 and goat anti-chicken Alexa Fluor 647, RRID:AB_2535866, all diluted 1:500 in PBS) were incubated at 37°C for 35 min. Slides were washed 3 × 5 min in 1X PBS and mounted with a 3:1 glycerol to PBS solution. Images were acquired at 10X on a Nikon E800 and merged in Affinity Photo (Serif, Nottingham, UK, RRID:SCR_016951) to obtain a full cross section. Merged images were analyzed for both fiber size and fiber type in MATLAB (Mathworks, Natick, MA, USA, RRID:SCR_001622) by semi-automatic muscle analysis using segmentation of histology (SMASH) software as previously described.²⁸

2.4.3 | NMJ staining and analyses

TA muscles from 10-month-old *Kmt2d*^{+/β^{Geo}} and WT mice were dissected and immediately fixed in 4% paraformaldehyde (PFA) in PBS for 2 h at 4°C. Muscles were then transferred into a 30% sucrose solution in PBS at 4°C overnight. Tissues were then placed longitudinally into plastic molds, embedded with OCT and frozen in liquid nitrogen-cooled isopentane. 50 μm transverse sections were cut

from the middle of the TA and post-fixed in cold (-20°C) methanol for 5 min, followed by a brief wash in ice-cold PBS. Sections were blocked in 10% goat serum with 0.1% Triton-X in 1X PBS for 1 h at RT. Primary antibody targeting neurofilament (2H3, DSHB, 1:50, RRID:AB_2618380) was diluted in blocking solution and incubated overnight at 4°C . Slides were washed 3×5 min in 1X PBS and incubated with secondary antibody 488-anti-Mouse IgG1 (1:500), and AlexaFluor594- α -bungarotoxin (B13423, ThermoFisher, Waltham, MA, USA, 1:250) diluted in 1X PBS for 1 h at RT. Following 3×5 min washes in 1X PBS, tissues were mounted and sealed. Images were acquired on a Zeiss LSM 700 Laser Scanning Confocal microscope (Zeiss, Oberkochen, Germany, RRID:SCR_017377) in the Boston Children's Hospital IDRC Imaging Core (RRID:SCR_012414). Only *en face* NMJs were selected, and Z-stacks were acquired $0.63 \mu\text{m}$ apart with pinhole set at 1.0 Airy unit. Images were analyzed using FIJI (NIH, Bethesda, MD, USA, RRID:SCR_002285) following a published protocol.²⁹ Area and perimeter were measured using the tracing tools in FIJI. The dispersion index was calculated as: total stained area/total area $\times 100$, indicating the density. After images were skeletonized, the FIJI plugin AnalyzeSkeleton was used to generate remaining parameters.²⁹

2.4.4 | Immunofluorescence detection of Pax7 and laminin

$8 \mu\text{m}$ frozen muscle tissue sections were fixed for 3 min in cold 100% methanol. Slides were rinsed in 1X PBS, then blocked for 45 min in 1X PBS with 10% fetal bovine serum. Sections were incubated overnight at 4°C with primary antibody (rabbit anti-laminin L9393 Sigma, St. Louis, MO, USA, RRID:AB_477163, diluted 1:1000 and anti-Pax7 concentrated supernatant, clone Pax7; Developmental Studies Hybridoma Bank, University of Iowa, Iowa City, IA, USA, RRID:AB_2299243) diluted 1:100 in blocking solution. The following day, slides were washed 4×5 min at RT in 1X PBS, incubated for 1 hr at RT in secondary antibodies (anti-mouse AlexaFluor594, RRID:AB_2632539, and anti-rabbit AlexaFluor488, Jackson ImmunoResearch, West Grove, PA, both diluted 1:500 in 1X PBS). Slides were washed again 4×5 min at RT in 1X PBS and mounted with Vectashield/DAPI before imaging. For each sample, entire sections were analyzed to count the number of Pax7+ cells and laminin-positive myofibers. The percentage of Pax7+ cells/total number of laminin-positive myofibers was calculated for each sample. The percentages of Pax7+ cells/myofibers were compared between control and KS-samples using an unpaired *t*-test (GraphPad Prism 9).

2.5 | Mouse muscle satellite cell isolation

Mouse muscle satellite cells were isolated using the MACS mouse Satellite Cell Isolation Kit (Miltenyi Biotec, Waltham, MA, USA), followed by positive selection for integrin- $\alpha 7$ expressing cells (Miltenyi Biotec, Waltham, MA, USA) as previously described.^{27,30} Briefly, skeletal muscle from WT and *Kmt2d*^{+/ β Geo} mice were dissected, minced, and dissociated with 5 mg/ml collagenase D and 1.2 U/ml dispase II for approximately 45 min at 37°C . After complete dissociation, tissue slurry was filtered through a $100 \mu\text{m}$ filter and centrifuged at 1200 rpm on a Beckman GH-3.8A rotor (Beckman Coulter, Brea, CA, USA) for 10 min. Red blood cell lysis was performed for 2 min at room temperature using Red Lysis Buffer (Qiagen, Hilden, Germany), filtered through a $40 \mu\text{m}$ filter and centrifuged again. MACS enrichment columns were used to deplete endothelial and fibro-adipogenic progenitors, followed by positive selection for integrin- $\alpha 7$ expressing cells, to enrich for satellite cells.²⁷ Satellite cell populations were plated on 6-well plates coated with ECL matrix in growth medium (Ham's F-10 supplemented with 20% FBS, 1x penicillin/streptomycin/glutamine (PSG) and 5 ng/ml bFGF).

2.6 | Myogenic differentiation assays

Equal numbers of myogenic cells ($n = 50\,000$) were plated in Permax 4-well chamber slides pre-coated with ECL attachment matrix following the manufacturer's guidelines (Millipore-Sigma, Burlington, MA, USA). Cells were maintained in differentiation medium, consisting of DMEM (1 g/L glucose) supplemented with 2% fetal bovine serum, 1X penicillin/streptomycin and 1X ITS supplement (GIBCO Thermo Fisher). Differentiation medium was changed daily for 5–7 days, after which cells were fixed in 2% PFA solution in PBS for 20 min at RT, rinsed in PBS and processed for immunofluorescence staining.

For immunostaining of myosin heavy chain, fixed cells were permeabilized for 5 min in 0.5% Triton-X solution in PBS and then rinsed once with 1X PBS. Slides were blocked for 45 min at room temperature in 1X PBS supplemented with 5% goat serum, then incubated overnight at 4°C with anti-myosin heavy chain (MHC supernatant, clone MF-20; Developmental Studies Hybridoma Bank, University of Iowa, Iowa City, IA, USA, RRID:AB_2147781) diluted 1:20 in 1X PBS or anti-myogenin (F5D concentrated supernatant, Developmental Studies Hybridoma Bank, University of Iowa, Iowa City, IA, USA, RRID:AB_2146602) diluted 1:100; or anti-MyoD (Santa Cruz, G1 733460, RRID:AB_2813894) diluted 1:200; or anti-Pax7 (concentrated supernatant, Developmental

Studies Hybridoma Bank, University of Iowa, Iowa City, IA, USA, RRID:AB_528428) diluted 1:100 together with anti-Ki-67 (Cell Signaling D3B5, RRID:AB_2687446), as previously described²⁷ diluted 1:500. The following day, slides were washed 4 × 5 min at RT in 1X PBS, incubated for 1 h at RT in secondary antibody (anti-mouse AlexaFluor594, RRID:AB_263254, diluted 1:500 in 1X PBS). Slides were washed again 4 × 5 min at RT in 1X PBS and mounted with Vectashield/DAPI before imaging. For each sample, entire chambers were counted for number of nuclei fused in MHC+ myotubes normalized over the total number of nuclei (fusion index); or the number of myogenin-positive nuclei divided by the total number of nuclei. Comparisons of fusion index and percentage of myogenin-positive cells between control and KS-samples were made using an unpaired *t*-test.

2.7 | Cardiotoxin injury and regeneration assays

Cardiotoxin injury in vivo was performed as previously described.²⁷ Briefly, anesthetized WT and *Kmt2d*^{+/β^{Geo} littermate male mice were injected in the belly of the right tibialis anterior (TA) with 15 μg of cardiotoxin per approved institutional protocols. Injured muscles were collected at 7 days post injury and frozen in cold isopentane for histological analyses. Sequential sections were taken to locate the injured area and immunostained with anti-laminin (rabbit anti-laminin L9393 Sigma, St. Louis, MO, USA, RRID:AB_477163, diluted 1:1000) and anti-embryonic myosin heavy chain (clone F1.652 from DSHB, 1:50, RRID:AB_528358). Images were stitched together using Affinity Photo (Serif, Nottingham, UK, RRID:SCR_016951) and fiber dimensions (minimum Feret's diameter and myofiber area) were measured using FIJI (NIH, Bethesda, MD, USA, RRID:SCR_002285).}

2.8 | Western blots

Skeletal muscle tissue was snap frozen and ground using a mortar and pestle precooled in liquid nitrogen. The tissue powder was resuspended in RIPA buffer with Protease and Phosphatase Inhibitor Cocktail Set III, EDTA Free (Millipore Sigma, Burlington, MA, USA). Lysates were sonicated for 3 × 5 s and spun at 13 000 RPM on a PRISM-R refrigerated microfuge to pellet tissue debris, while the supernatant was collected. Protein concentration was determined using PierceTM BCA protein assay kit (Thermo Scientific, Waltham, MA, USA). Samples were prepared with 4X NUPAGE loading buffer and 0.05% BME, boiled at 90°C for 10 min and spun again at 13 000

RPM, the supernatant was loaded onto a 4%–20% Tris-Glycine gel (BioRad, Hercules, CA, USA). Protein samples were run at 80 V for 10 min followed by 115V for 1 h on ice before being transferred to a PVDF membrane using a wet transfer system. Membranes were blocked for 1 h at room temperature in 5% BSA in TBS-0.1% Tween (TBST). Primary antibody against MEF2c (GeneTex, Irvine, CA, USA, RRID:AB_11173300; was diluted 1:1000 in TBST and incubated overnight at 4°C. Membranes were washed three times, 10 min each, with TBST at room temperature, hybridized with an HRP-Conjugated secondary antibody (Cell Signaling, Danvers, MA, USA, RRID:AB_2099233) for 1 h at room temperature, and washed with TBST three times for 10 min each. Detection of proteins probed with HRP-conjugated secondary was performed using Western Lightning[®] Plus-ECL Enhanced Chemiluminescence Substrate (Perkin Elmer, Waltham, MA, USA), blots were exposed on ProSignalTM Blotting Film (Prometheus Protein Biology Products, Genesee Scientific, San Diego, CA). To ensure equal loading of protein HRP-conjugated blots were stripped using RestoreTM Western Blot Stripping Buffer (Thermo Scientific, Waltham, MA, USA) and hybridized with anti-desmin (Abcam, Cambridge, MA, USA, RRID:AB_306653) using same HRP conjugated secondary and ECL. Optical density was measured FIJI (NIH, Bethesda, MD, USA, RRID:SCR_002285).

2.9 | In vivo cell transplantation into dystrophic mice

Freshly isolated 21 day old female *Kmt2d*^{+/β^{Geo} and WT satellite cells were resuspended in physiological grade sterile saline and injected intramuscularly into anesthetized immune-deficient, dystrophic Rag1^{null} *mdx*^{5cv} tibialis anterior (TA) muscles following procedures approved by the Boston Children's Hospital IACUC (protocol# 18-06-3730R). The mice were euthanized 10 weeks post-transplantation by CO₂ asphyxiation, followed by cervical dislocation, and the TA muscles were dissected and frozen for histology.²⁰ TA muscles from transplanted mice were serially sectioned at 8 μm to locate the transplant site. Frozen sections were then fixed in 100% methanol for 3 min, washed in cold 1X PBS once prior to incubation in blocking solution (PBS 10% fetal bovine serum) for 45 min at RT. Sections were incubated overnight at 4°C with anti-Dystrophin antibody CAP6-10,³¹ washed 4 × 5 min in 1X PBS and incubated with anti-rabbit Alexa-488 (Jackson ImmunoResearch, diluted 1:500, RRID:AB_2632534) for 1 h at room temperature. Following 4 × 5 min washes in 1X PBS, slides were mounted with Vectashield/DAPI (VectorLab, Burlingame, CA, USA). The injection sites were imaged with a fluorescent Nikon E800 microscope}

and SPOT software. The entire injection sites were reconstructed by stitching all images of dystrophin-positive myofibers and the total number of dystrophin-positive fibers was counted. For each animal, the total number of dystrophin-positive myofibers was used for statistical analyses.

3 | RESULTS

As hypotonia and fatigue have been described as clinical symptoms in KS patients,^{16–18} we performed muscle endurance studies on age- and sex-matched wildtype (WT) and *Kmt2d*^{+/β^{Geo}} mice to determine if the loss of *Kmt2d* drove

deficits in the skeletal muscle function. To study short-term muscle endurance and exercise capacity of our KS mouse strain, we employed the treadmill exhaustion test, where mice ran on a treadmill with increasing speed until exhaustion and the total distance run was measured.²⁶ Results from the treadmill test can reflect if there are muscular, cardiovascular, or neuromuscular issues within the mice. No significant difference in endurance was observed between WT and *Kmt2d*^{+/β^{Geo}} mice when comparing either male or female cohorts using a 2-way ANOVA (Figure 1A). Interestingly, while no significant difference was observed in running distance between males and females in WT cohorts, there was a sex-based difference in exercise capacity when analyzing the *Kmt2d*^{+/β^{Geo}}

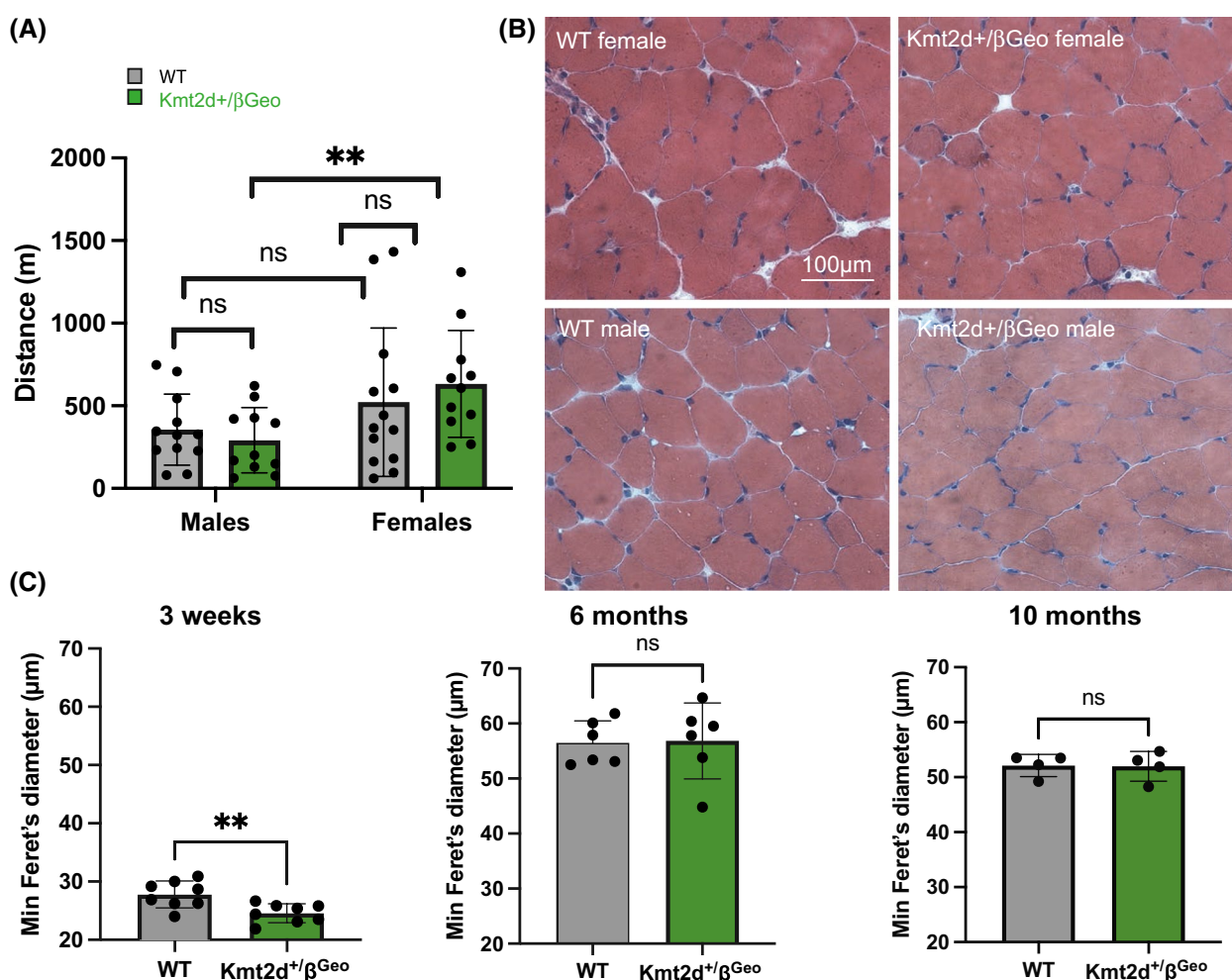


FIGURE 1 *Kmt2d*^{+/β^{Geo}} mice run similar distance as WT control mice and have smaller myofibers at weaning age. (A) Cohorts of age- and sex matched WT and *Kmt2d*^{+/β^{Geo}} mice were subjected to treadmill exhaustion tests and compared via 2-way ANOVA test. No significant difference in the distance run was observed when comparing WT and *Kmt2d*^{+/β^{Geo}} cohorts. Of note, *Kmt2d*^{+/β^{Geo}} female mice ran significantly longer than *Kmt2d*^{+/β^{Geo}} males. (B) H&E representative images of muscle tissue sections from WT and *Kmt2d*^{+/β^{Geo}} males and females, as indicated. (C) Minimum Feret's diameter was measured in equal groups of male and female mice at 3 weeks, 6 months and 10 months of age. Measurements were taken from thousands of myofibers/genotype from the entire sections of quadriceps muscles. Each dot represents the averaged Feret's diameter from one mouse. At 3 weeks, *Kmt2d*^{+/β^{Geo}} mice displayed significantly smaller myofibers compared to WT littermates. The deficiency was overcome at 6 and 10 months of age, where no significant difference in size was observed between *Kmt2d*^{+/β^{Geo}} and WT controls. *N* = 5–8 mice/group; ***p* < .01

genotype, where males ran a significantly shorter distance compared to females (Figure 1A). Following treadmill exercise, animals were euthanized and quadriceps and gastrocnemius muscles were dissected, frozen and analyzed in the same cohorts by H&E stain (Figure 1B). Myofiber size in WT and *Kmt2d*^{+/β^{Geo}} mice was assessed by measuring the minimum Feret's diameter in entire sections of quadricep muscle for each mouse. Measurement of the minimum Feret's diameter avoids any calculation bias of myofiber size when muscle fibers are not sectioned perfectly perpendicular to the cryostat blade. Examples of entire photomerged sections of male and female mice are shown in Figure S1A,B and violin plots displaying individual mouse measurements are shown in Figure S1C–E. At 3 weeks of age, *Kmt2d*^{+/β^{Geo}} mice displayed a significant reduction in myofiber size compared to WT littermates (Figure 1C). At 6 and 10 months of age, *Kmt2d*^{+/β^{Geo}} mice had overcome the initial deficit and no significant differences in fiber size were observed between the groups.

To investigate the biological mechanisms underlying the change in myofiber size in *Kmt2d*^{+/β^{Geo}} mice, tissue sections were immunostained for myosin proteins specifically expressed in slow (Type I and IIA) and fast-twitched (Type IIB) fibers. A recent study reported that myofiber-specific depletion of KMT2D leads to a decrease in MEF2C expression (a transcription factor involved in myogenic cell differentiation) and a decrease in slow Type I fibers in the soleus and gastrocnemius muscles.¹⁵ As slow Type I fibers are typically smaller in size and rich in mitochondria, their loss from slow muscles may result in a shift towards larger, Type IIB fibers, which, in turn, could explain the apparent increase in overall fiber size.¹⁵ To study whether the observed changes in fiber size in the *Kmt2d*^{+/β^{Geo}} model could be due to alterations in fiber type compositions (fast and slow), we examined the gastrocnemius muscle of male and female mice at 3 weeks of age. Tissue sections were immunostained for myosin proteins characteristic for slow- (Type I and IIA) and fast-twitch (Type IIX/IIB) fibers, using laminin as a marker to highlight the contour of myofibers (Figure 2A–D). Reconstructions of merged images of entire muscle sections are shown in Figure S2A and examples of violin plots of data collected for individual mice are shown in Figure S2B. The percentage of slow Type I fibers was significantly decreased in *Kmt2d*^{+/β^{Geo}} mice compared to WT controls (Figure 2E), in agreement with the previously reported data on the conditional model.¹⁵ Type IIA and IIX/IIB fibers, which collectively represented >95% of the muscle did not significantly differ in percentage between the genotypes (Figure 2E). We also performed comparisons of minimum Feret's diameter measurements based on myofiber type, but no significant changes were observed between the genotypes (Figure 2F). Further, western blot analysis

to quantify MEF2C expression in gastrocnemius muscle tissue lysates showed no significant changes in either females (Figure S2C,D) or males (Figure S2E,F).

To determine whether *Kmt2d*^{+/β^{Geo}} mice have potential abnormalities in nerve-muscle connection at the synapses, 10-month-old WT and *Kmt2d*^{+/β^{Geo}} male mice were histologically analyzed for morphological defects at the NMJs (Figure 3). The TA muscles were fixed and frozen longitudinally oriented, then serial 50μm sections were immunostained using an anti-neurofilament antibody to highlight the pre-synaptic nerve terminal and with α-bungarotoxin to define the post-synaptic acetylcholine-receptor dense-area (Figure 3A,B). More than 30 NMJs were analyzed for each genotype, which revealed no changes between WT and *Kmt2d*^{+/β^{Geo}} in the total post-synaptic stained area (Figure 3C), the dispersion index (Figure 3E, an indication of neuromuscular junction density), the number of post-synaptic branches (Figure 3F), the postsynaptic branch length (Figure 3G) and the myofiber diameter (Figure 3H). The only significant difference noted was decreased postsynaptic stained perimeter in *Kmt2d*^{+/β^{Geo}} animals compared to WT (Figure 3D). Thus, overall, *Kmt2d*^{+/β^{Geo}} mice displayed normal numbers and normal morphology in NMJ.

Muscle tissue from Kabuki patients has been scarcely studied and the consequences of mutations in *KMT2D* have not yet been elucidated. We obtained discarded skeletal muscle tissue from patients diagnosed with KS (*n* = 5) and with a confirmed pathogenic mutation in *KMT2D* (*n* = 4/5). Tissue sections were analyzed by H&E to detect any gross tissue abnormality (Figure 4A–C) and immunostained for fiber type composition (Type I, IIA, IIB, Figure 4D–F). Control muscle tissue sections from an unaffected adolescent individual displayed the typical regular pattern of muscle fibers closely located to one another (Figure 4A). Tissue samples from KS patients was suggestive of fibrotic infiltration, which was variably interspersed with muscle fiber fascicles (black arrows in Figure 4B,C). Sirius red staining was performed to confirm presence of fibrotic areas in KS muscle (Figure S3A,B) and presence of fibro-adipogenic progenitors was quantified following immunostaining for PDGFRα (Figure S3C–E), which appeared significantly increased in KS patient muscles compared to unaffected individuals. Measurements of myofiber size between control and KS samples by minimum Feret's diameter were not performed due to inconsistencies in age, gender and muscle type obtained from the patient and control groups, which are all variables known to affect myofiber size. Muscle fiber type compositions were analyzed in control and KS samples to determine whether a particular fiber type was under- or over- represented in the muscles. All fiber types were detected in control (Figure 4D) and KS samples (Figure 4E,F), with Type I and

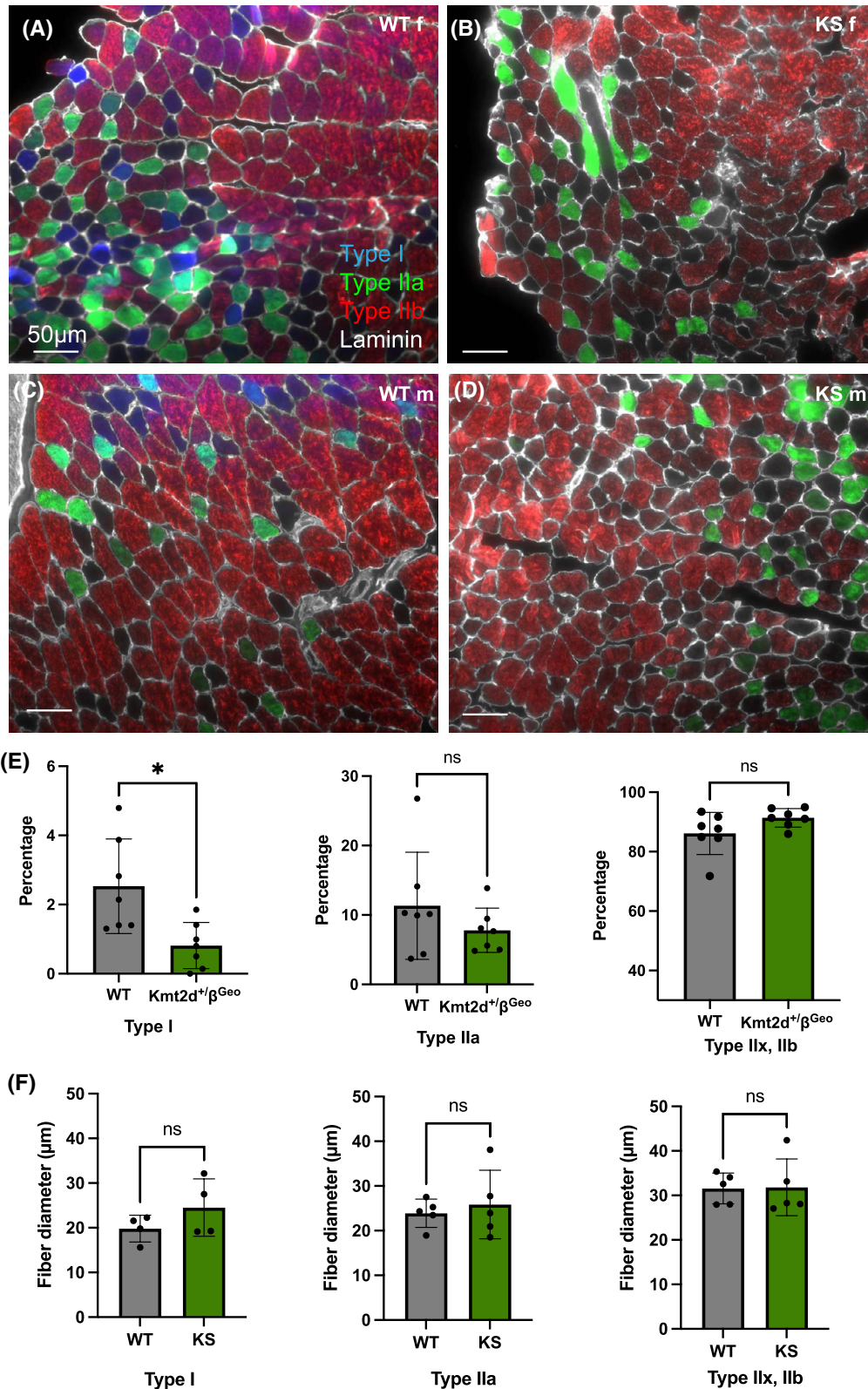


FIGURE 2 Quantification of fiber types in gastrocnemius muscle of WT and *Kmt2d*^{+/βGeo} mice. (A–D) Four-color immunofluorescence staining of 3 week old WT (A,C) and *Kmt2d*^{+/βGeo} (B, D) gastrocnemius muscles. A and B are muscles from littermate female mice while D and E are from littermate male mice. Laminin staining (grey) is used to highlight the contour of myofibers. Type I fibers are stained in blue, Type IIa fibers are stained in green, Type IIb fibers are stained in red. (E) Graphs showing the percentages of different fiber types in mouse cohorts. Each dot represents averaged data from an individual mouse. The percentage of type I (slow) fibers is significantly decreased in *Kmt2d*^{+/βGeo} mice. (F) Comparisons of minimum Feret's diameter of specific fiber types in WT and *Kmt2d*^{+/βGeo} mice show no significant difference in size. *N* = 4–7 mice/genotype; **p* ≤ .01

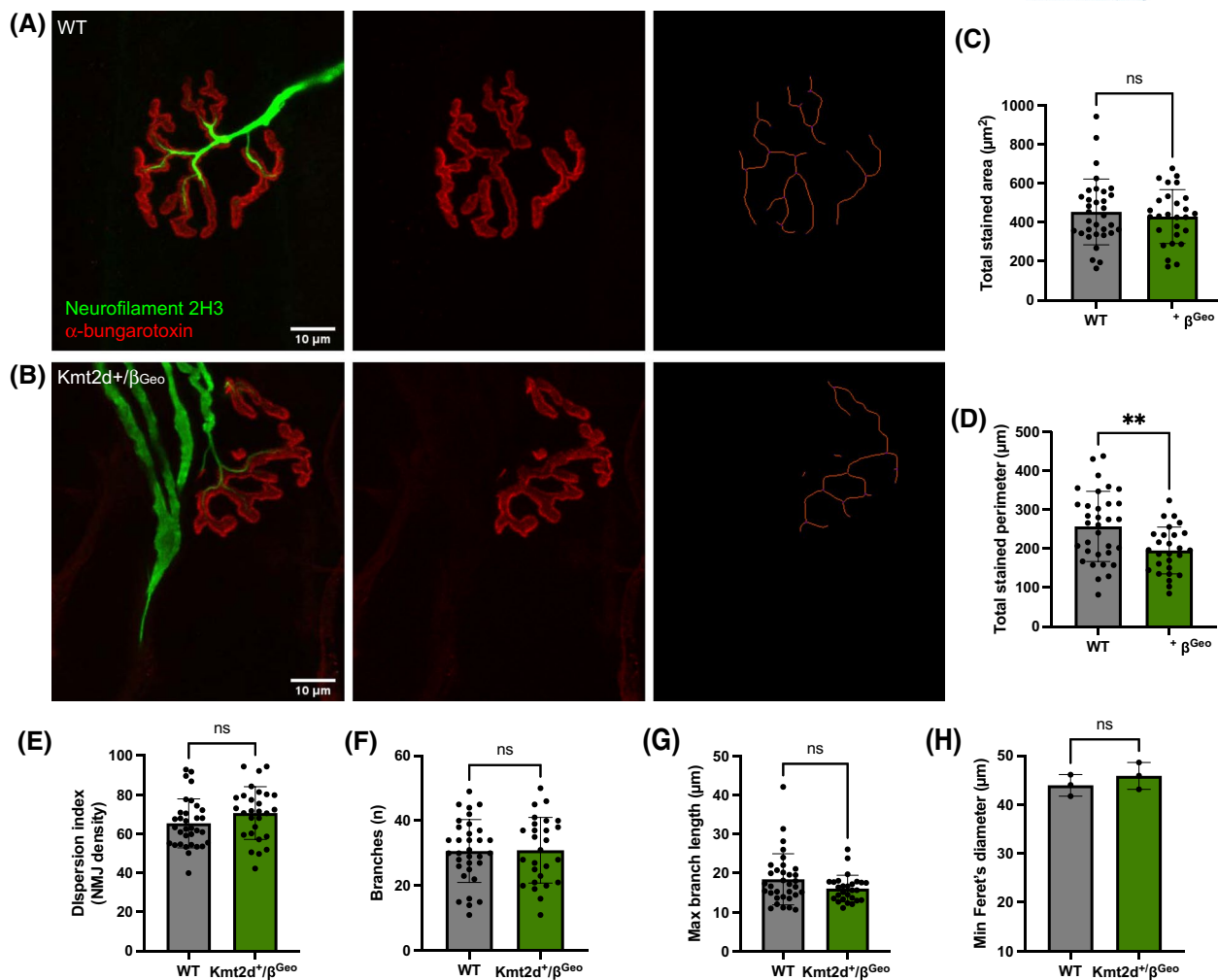


FIGURE 3 Neuromuscular junction analyses of WT and *Kmt2d*^{+/βGeo} mice. (A, B) Examples of pre-synaptic (neurofilament 2H3, green) and post-synaptic (α-bungarotoxin, red) fluorescent staining of 10-month old neuromuscular junctions of WT (A) and *Kmt2d*^{+/βGeo} male mice. The panel on the most right side in both (A) and (B) are examples of skeletonized images used to measure in Image J the number of branches (F) and maximum branch length (G). Images from 30 NMJ/genotype were analyzed in Image J and each dot represents data from a single NMJ. No significant differences were seen between WT and *Kmt2d*^{+/βGeo} mice in the total postsynaptic stained area (C), the dispersion index (E), which is the index of neuromuscular junction density; the number of post-synaptic branches (F) the maximum length of post-synaptic branches (G) or myofiber size of the TA muscle (H). A significant difference was noted in the post-synaptic total stained perimeter (D), which was decreased in *Kmt2d*^{+/βGeo} mice. ***p* ≤ .003

Type IIa fibers being the predominant types in KS samples (Figure 4G). Skeletal muscle is known to contain diverse types of progenitor cells, including fibro-adipogenic progenitors, muscle stem cells, also named satellite cells and endothelial progenitors.^{32,33} Intercellular signaling is known to play a role in maintaining a balance between skeletal muscle and fibrotic tissues,^{34,35} specifically muscle satellite cell activity is known to inhibit overproliferation of mesenchymal fibro-adipogenic progenitors.³⁶ Thus, we sought to determine whether the increased presence of fibrotic tissue observed in KS skeletal muscle might be triggered by a decreased number of muscle satellite cells or impaired satellite cell function. First, immunostaining for laminin and the muscle stem cell marker Pax7 were performed to locate and count muscle stem cells. Laminin

staining highlighted the myofiber contour and the extracellular space between myofibers, while Pax7 staining labeled nuclei of satellite cells (Figure 4H–J). The number of Pax7+ cells were counted in entire tissue sections (*n* = 4–5) for each sample and normalized to the number of myofibers in the section. Analyses of all KS and control samples concluded that the percentage of Pax7+ cells did not significantly differ between the groups (Figure 4K). Subsequently, myogenic cells were extracted from control and Kabuki samples as previously described^{21,22} and cultured in vitro to assess their myogenic activity. Equal number of cells were plated and differentiated for 5 days in low-serum media. Cells were then fixed and immunostained for myosin heavy chain (Figure 4L–N) and the fusion index was calculated by counting the number of

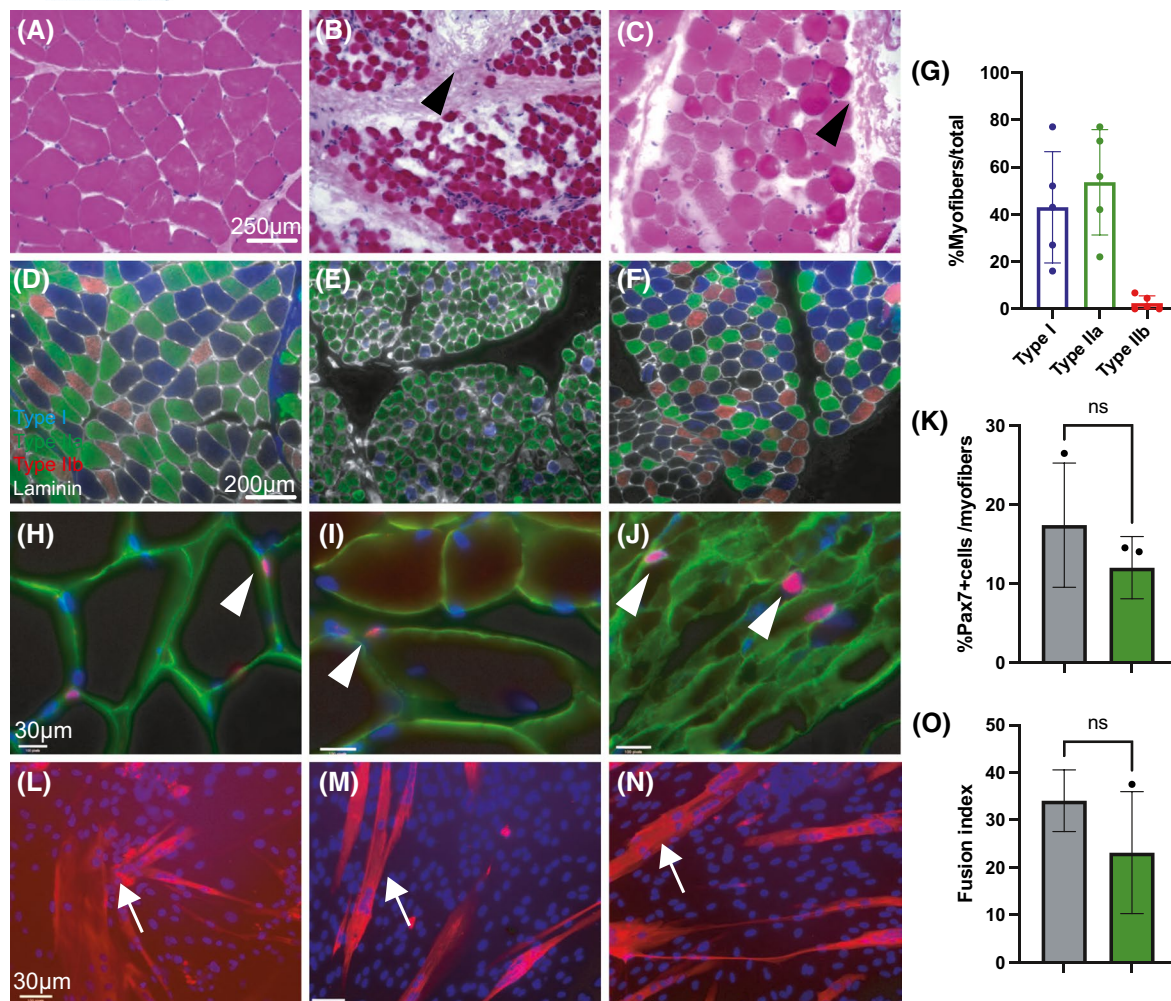


FIGURE 4 Histological analyses and muscle stem cell assessment in control and Kabuki syndrome human patient muscles. (A–C) H&E stains of control (A) and KS patient muscles (B, C). Both KS patients show presence of fibrotic tissue (black arrowheads) interspersed with myofiber bundles. (D–F) Fiber type analyses of control (D) and KS (E, F) muscles. Muscle fibers are stained in blue for Type I; green for Type IIa and red for Type IIb. Laminin staining (grey color) marks the myofiber contour. (G) Graph displaying fiber type composition of KS patient muscles ($n = 5$). Of note, Type I fibers are present in high proportions (average 40%), unlike what observed in *Kmt2d*^{+/β^{Geo} mice. (H–K) Immunostaining (H–J) and quantification (K) of the percentage of Pax7+ muscle satellite cells in muscle tissue sections. Muscle fibers are stained in green with laminin, while Pax7 expression is detected in red in the nuclei of muscle stem cells (white arrowheads). Nuclei are counterstained in blue with DAPI. The percentage of muscle stem cells is similar in control and KS patient tissues, suggesting muscle stem cell number is not affected in KS. (L–N) Muscle stem cells were extracted from control (L) and KS patient muscles (M, N) and induced to differentiate in vitro. Myotubes are stained in red with myosin heavy chain (MF20, white arrows). (O) Fusion index was calculated for control and KS samples, with no significant difference between the groups. Each dot in K and O represents averaged data obtained from one individual}

myogenic cells fused into myotubes over the total number of cells. While no statistically significant difference was seen between control and KS samples, a trend towards decreased fusion in KS samples was observed in 2 samples (Figure 4O).

To overcome the limitation of obtaining additional patient samples and the intrinsic variability associated with studies involving human samples, we sought to test whether myogenic cells from *Kmt2d*^{+/β^{Geo} animals exhibited differentiation defects in vitro. Muscle stem cells from control and *Kmt2d*^{+/β^{Geo} male and female mice ($n = 5$ –7/cohort)}}

were isolated and plated at equal density. After 48 h, cultures were immunostained for Pax7 and Ki67 to determine whether a difference in muscle stem cell activation might exist between the genotypes, which was not detected (Figure S3F, G). Confluent cultures were induced to differentiate to form myofibers in vitro. Immunostaining of myocytes/myotubes using MyoD, myogenin and MF20 (anti-myosin heavy chain) were performed to determine the differentiation potential of myogenic cells in vitro (Figure 5A–I). Immunostaining with anti-MyoD (Figure 5A–C) revealed that cultures from both genotypes were highly myogenic

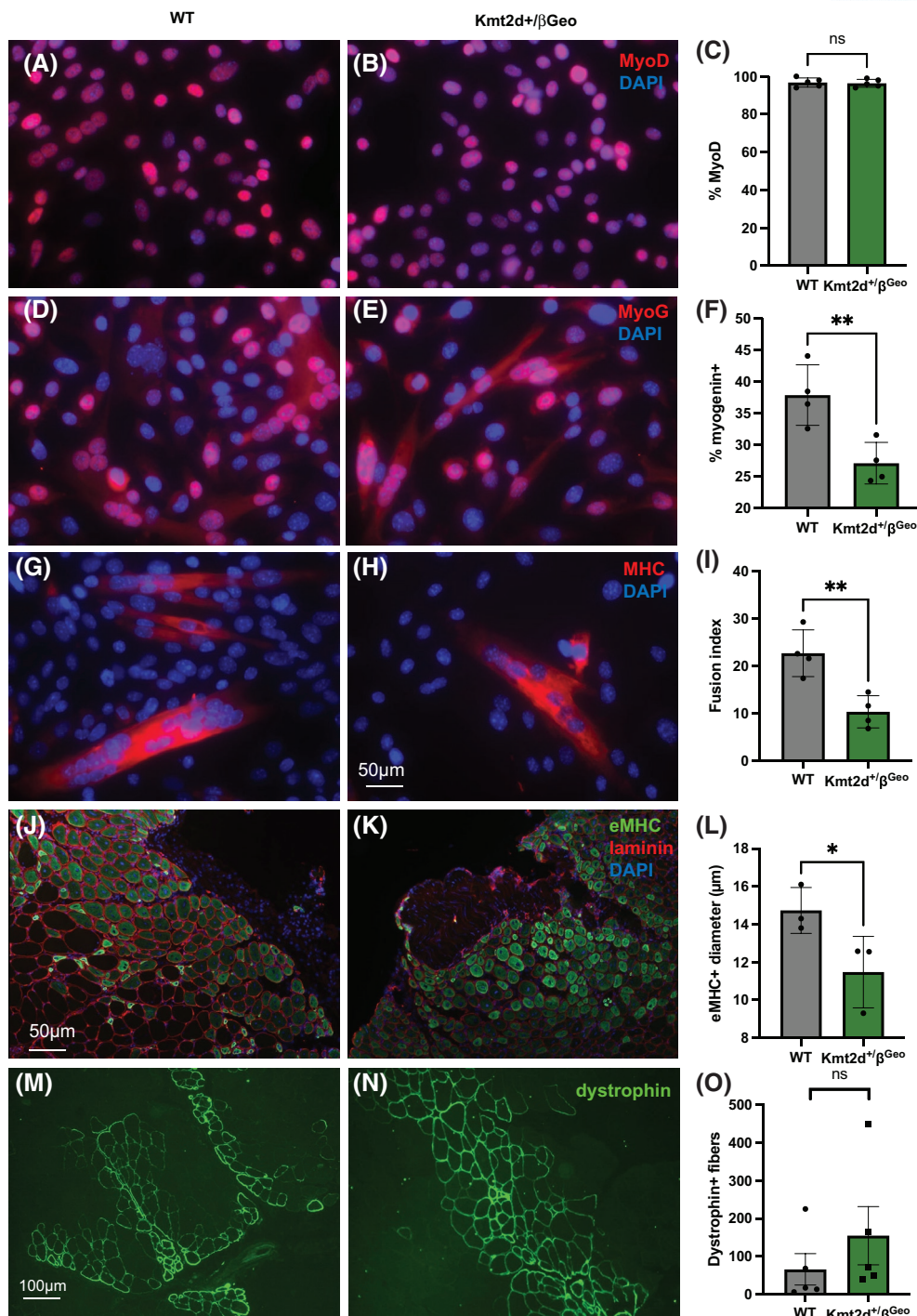


FIGURE 5 Muscle cells from *Kmt2d*^{+/βGeo} mice show decreased differentiation in vitro and in vivo, which is rescued when cells are transplanted in vivo in non-Kabuki muscle. (A–I) Immunostaining of WT and *Kmt2d*^{+/βGeo} confluent cell cultures using anti-MyoD (A, B), anti-myogenin (D, E) and anti-myosin heavy chain (G, H) following differentiation in vitro. (C) Quantification of MyoD-positive cells shown no significant difference in myogenic progenitors in the cultures. (F and I) Quantifications of myogenin-positive cells (F) and fusion index (I) show a significant decrease in myogenic differentiation in *Kmt2d*^{+/βGeo} samples (***p* ≤ .009). (J, K) Tissue sections of tibialis anterior muscles from WT (J) and *Kmt2d*^{+/βGeo} (K) male mice injured with cardiotoxin. After 7 days, muscles were collected and analyzed for presence and size of regenerating fibers. Myofiber contour is stained in red by laminin, while regenerating myofibers are stained in green with embryonic myosin (eMHC). (L) Quantification of fiber size indicated *Kmt2d*^{+/βGeo} regenerating fibers are significantly smaller compared to WT ones 7 days after injury (**p* = .03). Each dot in L represents averaged data from measurements taken from an individual mouse. (M, N) Examples of microscopic fields showing dystrophin expression (green) in *mdx*^{5cv} myofibers 10 weeks following transplantation of WT (M) or *Kmt2d*^{+/βGeo} (N) muscle stem cells. (O) Quantification of dystrophin-positive fibers following transplantation of WT and *Kmt2d*^{+/βGeo} cells show similar engraftment potential in vivo between the two genotypes, demonstrating that the differentiation defect of *Kmt2d*^{+/βGeo} cells can be overcome when cells are in a different environment

and there was no difference in the percentage of MyoD progenitors. Three days following induction of differentiation, the percentage of cells expressing myogenin was significantly decreased in *Kmt2d*^{+/β^{Geo}} cultures compared to WT ones (Figure 5D–F) and furthermore the fusion index was also significantly decreased in *Kmt2d*^{+/β^{Geo}} cultures compared to WT (Figure 5G–I). We then sought to determine whether *Kmt2d*^{+/β^{Geo}} primary myogenic cells exhibited decreased differentiation potential in vivo. To do this, we injured with cardiotoxin the tibialis anterior muscles of 4WT and 4*Kmt2d*^{+/β^{Geo}} male mice and assessed the size of regenerating myofibers 7 days post-injury. Muscles were immunostained with an antibody to embryonic myosin heavy chain (eMHC) (Figure 5J,K) and the size of regenerating fibers (minimum Feret's diameter) was assessed. *Kmt2d*^{+/β^{Geo}} mice displayed a significant decrease in regenerating myofiber size compared to WT littermates (Figure 5L, *p* < .03), confirming a delay in differentiation. Next, we determined whether the differentiation delays in *Kmt2d*^{+/β^{Geo}} muscle cells are irreversible, presumably due to the presence of repressive epigenetic marks at crucial muscle differentiation genes. Muscle satellite cells were purified from 3-week-old WT and *Kmt2d*^{+/β^{Geo}} female mice (*n* = 5/genotype) and immediately transplanted in equal numbers into the tibialis anterior (TA) muscle of recipient mice with muscular dystrophy (*Rag1*^{null}*mdx*^{5cv}), lacking the muscle protein dystrophin. In dystrophic mice, muscle fibers undergo spontaneous rounds of degeneration/regeneration and muscle stem cells are constantly recruited to repair damaged myofibers. Therefore, transplantation of donor WT or *Kmt2d*^{+/β^{Geo}} cells, which have a normal dystrophin gene, should result in fusion of these cells into dystrophic fibers and expression of dystrophin in the myofibers where donor cells have engrafted. Ten weeks following transplantation, TA muscles were harvested, serially sectioned and immunostained for dystrophin as an output measure to determine whether WT and *Kmt2d*^{+/β^{Geo}} muscle cells had similar differentiation/fusion potential in vivo (Figure 5M,N). Following image stitching and reconstruction of entire sections, the maximum number of dystrophin-positive fibers produced by injection of WT or *Kmt2d*^{+/β^{Geo}} muscle cells was quantified. No significant difference in the number of dystrophin-positive myofibers was seen between transplants of WT or mutant cells (*p* = .06, Figure 5O). These results suggest that any intrinsic deficiency of muscle stem cell differentiation in *Kmt2d*^{+/β^{Geo}} is reversible and can be corrected when the cells are placed in a non-Kabuki environment.

4 | DISCUSSION

Muscular hypotonia and fatigue are common symptoms observed in patients affected by KS, yet whether the

symptoms are due to primary deficiencies in neuronal or muscle tissue functions remains unclear. Our study focused on understanding whether loss of function of one allele of *Kmt2d* in mice and in patients affected by KS resulted in impaired differentiation of muscle stem cells, independent of neuronal function or whether abnormalities at the neuromuscular junction were present. Our analyses support the hypothesis that skeletal muscle is primarily affected due to a differentiation defect/delay in myogenic cells. This conclusion was underscored by multiple findings, both histologically and at a cellular function level. Histologically, no signs of muscle atrophy were observed in both human KMT2D patients and *Kmt2d*^{+/β^{Geo}} mice. Typically, loss of innervation results in grouping of angular shaped muscle fibers, termed grouped atrophy, which was not observed in our study in either mouse or human samples. Additionally, our analyses demonstrated that NMJs in mutant mice are present at a density similar to WT mice and that branching and size of postsynaptic areas are also normal in *Kmt2d*^{+/β^{Geo}} mice. Analyses of muscle fibers highlighted a decrease in myofiber size in young *Kmt2d*^{+/β^{Geo}} mice and in regenerating myofibers following acute injury. Myofiber size in skeletal muscle can be regulated by multiple mechanisms, which include differentiation/fusion of mononuclear myogenic cells into myotubes, as well as protein synthesis.^{37–39} Importantly, previous studies in mice demonstrated that muscle stem cell differentiation requires the function of the demethylase UTX/KDM6A, a gene also causative of KS¹⁹ and conditional loss of *Kdm6a* in muscle satellite cells resulted in impaired muscle regeneration in vivo.¹² Further, this impaired muscle regeneration was accompanied by decreased myofiber size and delayed differentiation of muscle cells into myotubes, caused by loss of activation of the transcription factor myogenin.¹² Our studies in myogenic cells from *Kmt2d*^{+/β^{Geo}} animals largely recapitulate the observations described for the *Kdm6a* model.¹² Indeed, our data showed decreased/delayed differentiation of muscle cells derived from *Kmt2d*^{+/β^{Geo}} animals due to decreased myogenin expression and decreased fusion in differentiating cultures, while MyoD expression did not differ. However, when muscle cells from *Kmt2d*^{+/β^{Geo}} animals were extracted and introduced into a dystrophic environment, where the primary defect is loss of the muscle structural protein dystrophin, mutant *Kmt2d*^{+/β^{Geo}} cells demonstrated similar abilities to differentiate and fuse into myofibers as WT cells. Thus, the epigenetic marks that presumably prevent muscle stem cell differentiation in *Kmt2d*^{+/β^{Geo}} environment can be 'erased' or modified when the cells are introduced into an environment where *Kmt2d* or *Kdm6a* are intact. These findings suggest that the deficiencies associated with heterozygous loss of *Kmt2d* might not

be permanent, but are potentially reversible, opening a potential avenue for therapeutic development.

The fatigue/exhaustion functional studies performed in *Kmt2d*^{+/β^{Geo} mice pointed to similar activity levels in mutant compared to WT mice. Interestingly, *Kmt2d*^{+/β^{Geo} female mice appeared to run a significantly longer distance compared to males. Differences in activity, particularly increased activity of female compared to male mice has been previously reported in other mouse studies and point to intrinsic differences between male and female mice that might not be connected to loss of function of specific genes.^{40–42} When measurements of fiber size were performed, *Kmt2d*^{+/β^{Geo} mice appeared to have significantly smaller fibers at 3 weeks of age, however these deficits were overcome at 6 and 10 months of age. Previous studies had documented that MEF2C expression, a target of KMT2D, affects specification of type I slow fibers, which are significantly reduced in mice with conditionally ablated *Kmt2d* expression in myofibers.¹⁵ Our studies in the *Kmt2d*^{+/β^{Geo} model support these conclusions, since a decreased percentage of type I slow fibers was also observed in our mutant mice, however we did not detect differences in expression of MEF2C. Interestingly, recent observations in a new *Kmt2d* model reports increased general activity, distance traveled and average speed in mutant mice,¹⁴ suggesting some similarities to what we observed in the *Kmt2d*^{+/β^{Geo} model.}}}}}

Our studies also analyzed skeletal muscle samples from KS patients, where samples displayed presence of increased fibrosis that was not observed in *Kmt2d*^{+/β^{Geo} mice, pointing to some potential differences between mouse models and human disease. Second, our studies showed robust presence of Type I fibers in all KS muscles analyzed, another difference when compared to the mouse model. Thirdly, when muscle cells from KS patients were differentiated, a variable reduction in differentiation was observed. These results highlight the need to continue the analyses on additional patient samples to increase our understanding of the common downstream mechanisms affected by loss of KMT2D function, regardless of where the primary mutation is located. In addition, correlation of functional defects or abnormalities with the genotype may advance our understanding of specific KMT2D protein domain function.}

In summary, our studies in human and mouse muscles emphasize the value of parallel analyses in both species to better define similarities and differences in the models. Such studies will strengthen our ability to design translatable pre-clinical experiments in disease models that allow for more reliable predictions of response to drug candidates in humans. These studies will open new avenues towards identification and testing of effective therapies that can ameliorate symptoms associated with human disease.

ACKNOWLEDGMENTS

The authors would like to thank all patients and families who participated in this study. The Pax7, F5D (myogenin), eMHC (clone F1.652) and MHC (MF20) antibodies were obtained from the Developmental Studies Hybridoma Bank, created by the NICHD of the NIH and maintained at The University of Iowa, Department of Biology, Iowa City, IA 52242. This work was supported by private donations to the Royce Kabuki Program at Boston Children's Hospital.

DISCLOSURES

The authors have no conflicts of interest to declare.

AUTHOR CONTRIBUTIONS

Alec Wright and Emanuela Gussoni designed research, performed research, analyzed data and wrote the paper; Arielle Hall designed research, performed research and analyzed data; Tatiana Fontelonga, Sarah Potter, Caitlin Schafer, and Andrew Lindsley performed research and analyzed data; Tara Daly, Christina Hung and Olaf Bodamer contributed new reagents and analyzed data.

ORCID

Emanuela Gussoni  <https://orcid.org/0000-0002-9915-3677>

REFERENCES

1. Sobreira N, Brucato M, Zhang L, et al. Patients with a Kabuki syndrome phenotype demonstrate DNA methylation abnormalities. *Eur J Hum Genet.* 2017;25:1335–1344.
2. Dorigi KM, Swigut T, Henriques T, et al. Mll3 and Mll4 facilitate enhancer RNA synthesis and transcription from promoters independently of H3K4 monomethylation. *Mol Cell.* 2017;66:568–576.e564.
3. Rickels R, Herz HM, Sze CC, et al. Histone H3K4 monomethylation catalyzed by Trr and mammalian COMPASS-like proteins at enhancers is dispensable for development and viability. *Nat Genet.* 2017;49:1647–1653.
4. Dhar SS, Lee SH, Chen K, et al. An essential role for UTX in resolution and activation of bivalent promoters. *Nucleic Acids Res.* 2016;44:3659–3674.
5. Shpargel KB, Starmer J, Wang C, Ge K, Magnuson T. UTX-guided neural crest function underlies craniofacial features of Kabuki syndrome. *Proc Natl Acad Sci U S A.* 2017;114:E9046–E9055.
6. Adam MP, Banka S, Bjornsson HT, et al. Kabuki syndrome: international consensus diagnostic criteria. *J Med Genet.* 2019;56:89–95.
7. Goo YH, Sohn YC, Kim DH, et al. Activating signal cointegrator 2 belongs to a novel steady-state complex that contains a subset of trithorax group proteins. *Mol Cell Biol.* 2003;23:140–149.
8. Lee JE, Wang C, Xu S, et al. H3K4 mono- and dimethyltransferase MLL4 is required for enhancer activation during cell differentiation. *eLife.* 2013;2:e01503.
9. Froimchuk E, Jang Y, Ge K. Histone H3 lysine 4 methyltransferase KMT2D. *Gene.* 2017;627:337–342.

10. Jang Y, Wang C, Zhuang L, Liu C, Ge K. H3K4 methyltransferase activity is required for MLL4 protein stability. *J Mol Biol.* 2017;429:2046-2054.
11. Bjornsson HT, Benjamin JS, Zhang L, et al. Histone deacetylase inhibition rescues structural and functional brain deficits in a mouse model of Kabuki syndrome. *Sci Transl Med.* 2014;6:256ra135.
12. Faralli H, Wang C, Nakka K, et al. UTX demethylase activity is required for satellite cell-mediated muscle regeneration. *J Clin Invest.* 2016;126:1555-1565.
13. Carosso GA, Boukas L, Augustin JJ, et al. Precocious neuronal differentiation and disrupted oxygen responses in Kabuki syndrome. *JCI Insight.* 2019;4:129375.
14. Yamamoto PK, de Souza TA, Antiorio A, et al. Genetic and behavioral characterization of a Kmt2d mouse mutant, a new model for Kabuki Syndrome. *Genes Brain Behav.* 2019;18:e12568.
15. Liu L, Ding C, Fu T, et al. Histone methyltransferase MLL4 controls myofiber identity and muscle performance through MEF2 interaction. *J Clin Invest.* 2020;130:4710-4725.
16. Kuroki Y, Suzuki Y, Chyo H, Hata A, Matsui I. A new malformation syndrome of long palpebral fissures, large ears, depressed nasal tip, and skeletal anomalies associated with postnatal dwarfism and mental retardation. *J Pediatr.* 1981;99:570-573.
17. Schrandt-Stumpel CT, Spruyt L, Curfs LM, Defloor T, Schrandt JJ. Kabuki syndrome: clinical data in 20 patients, literature review, and further guidelines for preventive management. *Am J Med Genet A.* 2005;132A:234-243.
18. Miyake N, Koshimizu E, Okamoto N, et al. MLL2 and KDM6A mutations in patients with Kabuki syndrome. *Am J Med Genet A.* 2013;161A:2234-2243.
19. Seenundun S, Rampalli S, Liu QC, et al. UTX mediates demethylation of H3K27me3 at muscle-specific genes during myogenesis. *EMBO J.* 2010;29:1401-1411.
20. Meng H, Janssen PM, Grange RW, et al. Tissue triage and freezing for models of skeletal muscle disease. *J Vis Exp.* 2014;89:51586.
21. Spinazzola JM, Gussoni E. Isolation of primary human skeletal muscle cells. *Bio Protoc.* 2017;7:2591.
22. Pakula A, Spinazzola JM, Gussoni E. Purification of myogenic progenitors from human muscle using fluorescence-activated cell sorting (FACS). *Methods Mol Biol.* 2019;1889:1-15.
23. Benjamin JS, Pilarowski GO, Carosso GA, et al. A ketogenic diet rescues hippocampal memory defects in a mouse model of Kabuki syndrome. *Proc Natl Acad Sci U S A.* 2017;114:125-130.
24. Fahrner JA, Lin WY, Riddle RC, et al. Precocious chondrocyte differentiation disrupts skeletal growth in Kabuki syndrome mice. *JCI Insight.* 2019;4:129380.
25. Chal J, Oginuma M, Al Tanoury Z, et al. Differentiation of pluripotent stem cells to muscle fiber to model Duchenne muscular dystrophy. *Nat Biotechnol.* 2015;33:962-969.
26. Schafer C, Moore V, Dasgupta N, et al. The effects of PPAR stimulation on cardiac metabolic pathways in Barth syndrome mice. *Front Pharmacol.* 2018;9:318.
27. Hall A, Fontelonga T, Wright A, et al. Tetraspanin CD82 is necessary for muscle stem cell activation and supports dystrophic muscle function. *Skelet Muscle.* 2020;10:34.
28. Smith LR, Barton ER. SMASH—semi-automatic muscle analysis using segmentation of histology: a MATLAB application. *Skelet Muscle.* 2014;4:21.
29. Pratt SJP, Shah SB, Ward CW, Inacio MP, Stains JP, Lovering RM. Effects of in vivo injury on the neuromuscular junction in healthy and dystrophic muscles. *J Physiol.* 2013;591:559-570.
30. Sacco A, Doyonnas R, Kraft P, Vitorovic S, Blau HM. Self-renewal and expansion of single transplanted muscle stem cells. *Nature.* 2008;456:502-506.
31. Lidov HG, Byers TJ, Watkins SC, Kunkel LM. Localization of dystrophin to postsynaptic regions of central nervous system cortical neurons. *Nature.* 1990;348:725-728.
32. Baghdadi MB, Tajbakhsh S. Regulation and phylogeny of skeletal muscle regeneration. *Dev Biol.* 2018;433:200-209.
33. Wosczyzna MN, Rando TA. A muscle stem cell support group: coordinated cellular responses in muscle regeneration. *Dev Cell.* 2018;46:135-143.
34. Joe AW, Yi L, Natarajan A, et al. Muscle injury activates resident fibro/adipogenic progenitors that facilitate myogenesis. *Nat Cell Biol.* 2010;12:153-163.
35. Natarajan A, Lemos DR, Rossi FM. Fibro/adipogenic progenitors: a double-edged sword in skeletal muscle regeneration. *Cell Cycle.* 2010;9:2045-2046.
36. Uezumi A, Fukada S, Yamamoto N, Takeda S, Tsuchida K. Mesenchymal progenitors distinct from satellite cells contribute to ectopic fat cell formation in skeletal muscle. *Nat Cell Biol.* 2010;12:143-152.
37. Berdeaux R, Stewart R. cAMP signaling in skeletal muscle adaptation: hypertrophy, metabolism, and regeneration. *Am J Physiol Endocrinol Metab.* 2012;303:E1-E17.
38. Pallafacchina G, Blaauw B, Schiaffino S. Role of satellite cells in muscle growth and maintenance of muscle mass. *Nutr Metab Cardiovasc Dis.* 2013;23(suppl 1):S12-S18.
39. Roberts MD, Haun CT, Mobley CB, et al. Physiological differences between low versus high skeletal muscle hypertrophic responders to resistance exercise training: current perspectives and future research directions. *Front Physiol.* 2018;9:834.
40. Rezende EL, Kelly SA, Gomes FR, Chappell MA, Garland T Jr. Effects of size, sex, and voluntary running speeds on costs of locomotion in lines of laboratory mice selectively bred for high wheel-running activity. *Physiol Biochem Zool.* 2006;79:83-99.
41. Bartling B, Al-Robaiy S, Lehnich H, Binder L, Hiebl B, Simm A. Sex-related differences in the wheel-running activity of mice decline with increasing age. *Exp Gerontol.* 2017;87:139-147.
42. Zhou CN, Chao FL, Zhang Y, et al. Sex differences in the white matter and myelinated fibers of APP/PS1 mice and the effects of running exercise on the sex differences of AD mice. *Front Aging Neurosci.* 2018;10:243.

SUPPORTING INFORMATION

Additional supporting information may be found in the online version of the article at the publisher's website.

How to cite this article: Wright A, Hall A, Daly T, et al. Lysine methyltransferase 2D regulates muscle fiber size and muscle cell differentiation. *FASEB J.* 2021;35:e21955. doi:[10.1096/fj.20210823R](https://doi.org/10.1096/fj.20210823R)